ARTICLE

Check for updates

Direct energy transfer from photosystem II to photosystem I confers winter sustainability in Scots Pine

Pushan Bag [1,8], Volha Chukhutsina[2,5,8], Zishan Zhang[1,7], Suman Paul[1,6], Alexander G. Ivanov [3,4], Tatyana Shutova[1], Roberta Croce [2], Alfred R. Holzwarth [2✉] & Stefan Jansson [1✉]

Evergreen conifers in boreal forests can survive extremely cold (freezing) temperatures during long dark winter and fully recover during summer. A phenomenon called "sustained quenching" putatively provides photoprotection and enables their survival, but its precise molecular and physiological mechanisms are not understood. To unveil them, here we have analyzed seasonal adjustment of the photosynthetic machinery of Scots pine (*Pinus sylvestris*) trees by monitoring multi-year changes in weather, chlorophyll fluorescence, chloroplast ultrastructure, and changes in pigment-protein composition. Analysis of Photosystem II and Photosystem I performance parameters indicate that highly dynamic structural and functional seasonal rearrangements of the photosynthetic apparatus occur. Although several mechanisms might contribute to 'sustained quenching' of winter/early spring pine needles, time-resolved fluorescence analysis shows that extreme down-regulation of photosystem II activity along with direct energy transfer from photosystem II to photosystem I play a major role. This mechanism is enabled by extensive thylakoid destacking allowing for the mixing of PSII with PSI complexes. These two linked phenomena play crucial roles in winter acclimation and protection.

[1] Umeå Plant Science Centre, Department of Plant Physiology, Umeå University, Umeå, Sweden. [2] Department of Physics and Astronomy, Faculty of Sciences, Vrije Universiteit Amsterdam, Amsterdam, The Netherlands. [3] Department of Biology, University of Western Ontario, London, Ontario, Canada. [4] Institute of Biophysics and Biomedical Engineering, Bulgarian Academy of Sciences, Sofia, Bulgaria. [5] Present address: Department of Life Sciences, Imperial College London, London, UK. [6] Present address: Department of Biochemistry and Biophysics, Stockholm University, Stockholm, Sweden. [7] Present address: State Key Laboratory of Crop Biology, College of Life Sciences, Shandong Agricultural University, Shandong, China. [8] These authors contributed equally: Pushan Bag, Volha Chukhutsina. ✉email: a.holzwarth@vu.nl; stefan.jansson@umu.se

Photosynthesis is the basis for most life on earth, and the ability to sustain growth by harvesting sunlight confers such an enormous evolutionary advantage that photosynthetic organisms have developed numerous adaptations that enable them to photosynthesize in diverse environments. These include vast boreal forests, which cover ~70% of all coniferous forests of the world (mainly in the northern hemisphere)[1], which have lower species diversity than many other terrestrial ecosystems and are often dominated by evergreen conifers, like pine and spruce[2]. Broadleaf deciduous trees and shrubs are also present, and sometimes deciduous conifers such as Larch (*Larix*) species, but there is no doubt that evergreen conifers are particularly well adapted to harsh boreal conditions, including short growing seasons and cold, snowy winters. Thus, evergreen conifers acclimations to boreal regions must presumably include regulatory processes that protect the photosynthetic apparatus in their needles during the harsh winter and early spring. Knowledge of photoprotective mechanisms in various kinds of photosynthetic organisms has increased considerably in recent decades. Several control systems have been identified that allow the photosynthesis machinery to harmlessly dissipate excess excitation energy[3–7]. In 2003, Öquist and Huner[8] published a seminal review of photosynthesis in evergreen plants, which pointed out that over-wintering conifer needles enter a state of 'sustained quenching' during winter. They found strong evidence for major alterations in the organization and composition of the photosystem II (PS II) antenna but also concluded that photosystem I (PS I) may play an important role, via nonphotochemical quenching of absorbed light or via quenching absorbed light photochemically through cyclic electron transport. Recently it was also shown that alternative electron transport might add up to this as well[9]. Up to date, there exists no clear mechanism rationalizing winter quenching in conifers although there are several proposed hypotheses[8,10]. Several protection mechanisms may also occur in parallel and (if so) they are likely activated largely well before the extreme stress occurs[11,12]. But the major conundrum arises in early spring, when temperatures are typically still low, so plants' biochemical and metabolic activities are strongly limited, but solar radiation is already high[8]. Once induced, the mechanisms need to be sustained, i.e., locked-in over the long winter season and protect the photosynthetic machinery. When conditions improve late in the spring, photosynthetic apparatus is restored and attains its active growth state in summer.

In previous explorations of these phenomena, a marked drop in Photosystem II photochemistry (measured as Fv/Fm) has been recorded in several overwintering conifers, and some indications of the quenching mechanisms involved have been suggested. These reportedly include destacking of thylakoid membranes and associated changes in chloroplast ultrastructure[13], in accordance with the drop in PSII maximal fluorescence[8]. In higher plants, thylakoid stacking and heterogeneity play crucial roles in the localizations of PSII and PSI in grana (tightly appressed thylakoid layers) and stroma lamellae, respectively. In conifers, although an extreme drop in maximal fluorescence (Fm) in winter/early spring has been observed, its mechanistic relationship to thylakoid structural changes has not been explained. It was recently shown that phosphorylation of PsbS and Lhcb1 might be a prerequisite for this phenomenon in spruce[14], triple phosphorylation of Lhcb1 was linked with massive destacking of thylakoids but its physiological relevance was yet undefined. In the study reported here we monitored steady-state chlorophyll fluorescence, ultrafast time-resolved fluorescence, and chloroplast ultrastructure in Scots pine needles from autumn to summer in three successive years. Our data strongly indicate that chlorophyll fluorescence quenching and thylakoid destacking are strongly linked, mutually dependent and crucial for the survival of evergreen conifers in the extreme northern boreal winter and early spring, when temperatures are low but solar radiation levels may be high.

Results

Seasonal changes in Photosystem II- and Photosystem I-related functional activities. To monitor photosynthetic performance, we recorded several PSII and PSI parameters during three consecutive growth seasons (2015–2016, 2016–2017, and 2017–2018) along with concomitant changes in daily air temperature and solar radiation (Fig. 1a–c). For simplicity, in the main figures we only present (here onwards) data from 2017 to 2018, which we divided into five distinct seasons, based on weather parameters: Summer (S, June–Aug), autumn (A, Sept–mid Nov), winter (W, mid Nov–mid Feb), early spring (ES, mid Feb–mid Apr), and late spring (LS, mid Apr–June). Data from the other two growth seasons are provided in Supplementary Figs. 1–3.

We found characteristic seasonal patterns in maximum PSII fluorescence (Fm) and maximum quantum efficiency of PSII (expressed as Fv/Fm), in accordance with earlier reports[8,10]. Fv/Fm was highest in S, fell with reductions in ambient temperatures during A and W (Fig. 1d, e), and was lowest in ES (63% lower than in S), when low temperatures coincided with rises in solar irradiance (Fig. 1a–c; see also Supplementary Fig. 2a). During LS, Fv/Fm gradually increased with increasing temperatures and peaked in S. The seasonal changes recorded in Fv/Fm were found to be mostly affected by changes in Fm rather than Fo (basic intrinsic fluorescence) (Fig. 1d). For a deeper understanding of PSII performance, the fraction of absorbed light energy utilized by PSII photochemistry[15] (ΦPSII) was measured (Fig. 1f). During W ΦPSII decreased significantly and reached minimal values (19% of S values) in ES (Supplementary Fig. 2b).

Furthermore, we tried to quantify the amount of absorbed light energy thermally dissipated by non-photochemical quenching (NPQ)[3]. The component of NPQ that play a crucial role under fluctuating light conditions is the fast component (ΔpH-PsbS dependent-qE[3] or zeaxanthin dependent-qZ[4]), which increased with increasing light intensities in all the seasons. In S and A, the fast component did not reach a stationary phase even at 1500 μmol m^{-2} s^{-1} illumination, while in W and LS samples a stationary phase was reached at 500 μmol m^{-2} s^{-1} and in ES already at 300 μmol m^{-2} s^{-1} (Fig. 1g). Most importantly, in ES inducible steady-state NPQ was much smaller and overall slower due to the smaller amplitude of the fast component (~50% less than in S) in ES (Fig. 1h). This is due to the fact that ES needles have already developed static NPQ. Instead, the quantum yield of non-regulated and/or constitutive loss (ΦNO) of energy was high during ES (Fig. 1i) (Supplementary Fig. 2d). This strongly suggests that this static NPQ is the fraction of absorbed light energy neither going to drive photochemistry (Φ$_{PSII}$) nor thermally dissipated by rapid regulated NPQ processes (qE/qZ).

To confirm that this static quenching is a manifestation of a "sustained mode of quenching" we artificially relaxed the ES needles (hereafter, ER) for 48 h in low light (80 μmol m^{-2} s^{-1}) with 18/6 h photoperiod. During this recovery, we observed no significant changes in Fv/Fm for 6–8 h (less than a 10% increase), a modest increase (30%) after 24 h (Fig. 1j), and almost complete (95%) recovery to S levels after 48 h. Fo did not change significantly throughout the recovery period (Fig. 1j), but changes in Fm followed the same recovery dynamics as Fv/Fm (Fig. 1j), although maximal fluorescence (Fm) was much higher in S than in 48 h ER samples. ΦPSII did not change significantly until 12 h of recovery but recovered to 50% and 90% of S levels after 24 and 48 h, respectively (Fig. 1k). qE/qZ-dependent fast NPQ kinetics followed similar patterns to ΦPSII (Fig. 1l). It should be noted that light-dependent induction of the fast component of NPQ
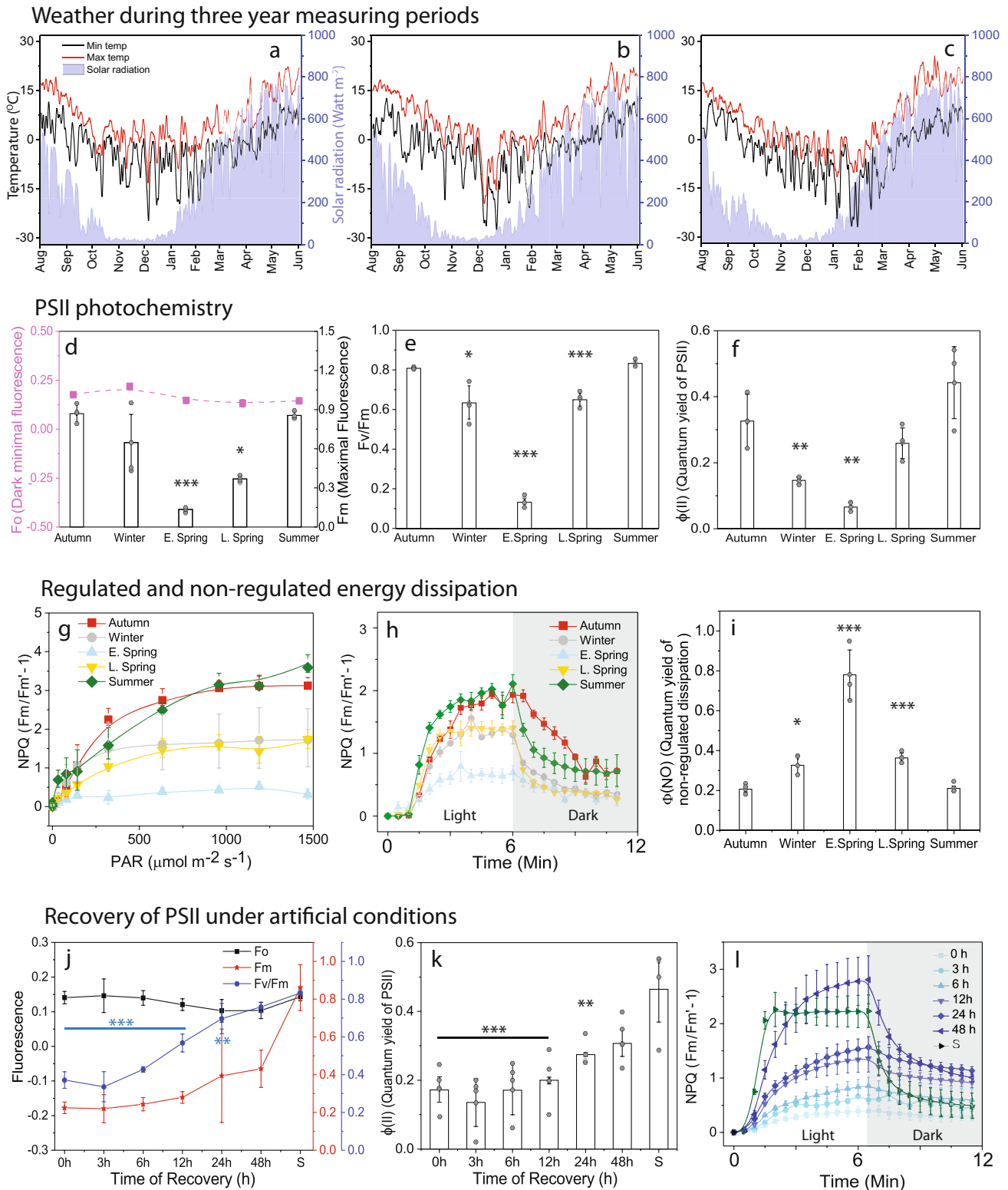
Fig. 1 Seasonal dynamics of weather and photochemical performance of PSII measured by chlorophyll fluorescence in Scots pine needles. Changes in temperature (°C) (Left Y-axis) and solar radiation (watt m^{-2}) (Right Y-axis) during 2015–2016 (**a**), 2016–2017 (**b**), 2017–2018 (**c**) measuring seasons. Seasonal dynamics of PSII photochemistry: (**d**) Changes in maximal (Fm) and basic (Fo) fluorescence. (**e**) Maximal quantum efficiency of PSII measured as Fv/Fm (**f**) Effective quantum yield of PSII (Φ(II)). Energy dissipation measured as regulated and non-regulated non-photochemical quenching: (**g**) Changes in NPQ with increasing PAR. (**h**) Induction of NPQ with constant actinic light. (**i**) Quantum yield of non-regulated non-photochemical quenching. Recovery of pine needles under artificial conditions at 80 μmol photons m^{-2} s^{-1} of light for 48 h with 18/6 photoperiod: (**j**) Changes in Fo. Fm and Fv/Fm. (**k**) Changes in Φ(II). (**l**) Induction of NPQ with constant actinic light. Quantum yields were calculated at actinic light illumination of 300 μmol m^{-2} s^{-1} in the light response curve and NPQ induction was measured either at 300/800 μmol m^{-2} s^{-1} of actinic light illumination. All measurements were taken after 30 min of dark adaptation at 4 °C from winter to late spring and room temperature in summer. Error bars indicate the mean ± SD (n = 3) for (**d**–**g**), and (**i**); ± SD (n = 4) for (**j**, **k**). Error bars indicate the mean ± SE (n = 3) for (**h**, **l**). The statistically significant mean differences (t-test) are marked by asterisks indicating the following confidence intervals: *≤95%; **≤99%.; ***≤99.9%. Exact p values are provided in the source data file.
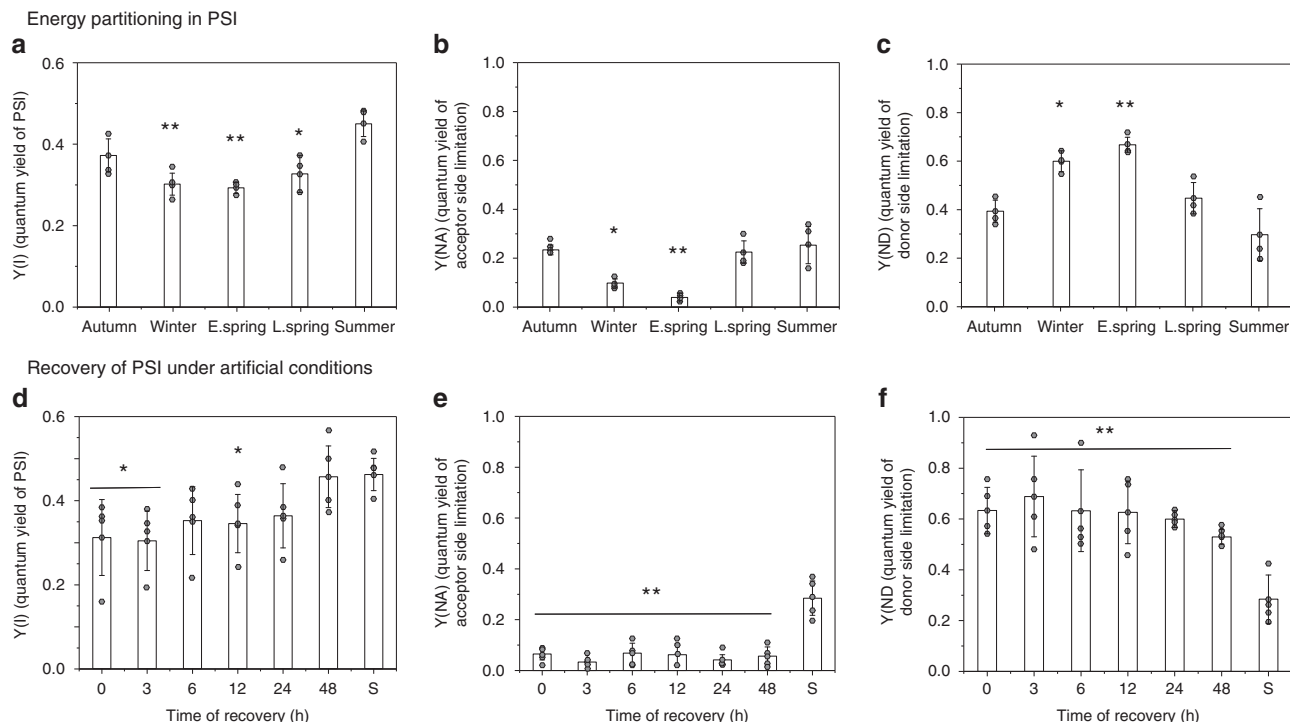
Fig. 2 Seasonal changes of PSI photochemistry in Scots pine needles. Energy partitioning in PSI considering Y(I) + Y(ND) + Y(NA) = 1, where Y(I) (**a**), Y(NA) (**b**), Y(ND) (**c**) are the photochemical quantum yield of PSI (when P700 is reduced and A is oxidized), energy dissipation in PSI (a measure of acceptor side limitation, when P700 and A both are reduced) and energy dissipation in PSI (a measure of donor side limitation, when P700 and A both are oxidized), respectively. Recovery of PSI photochemistry under artificial conditions: (**d**) Y(I), (**e**) Y(NA), (**f**) Y(ND) of PSI during the recovery period. Quantum yields were calculated from 300 µmol m^{-2} s^{-1} light illumination period of a light response curve. All measurements were taken after 30 min of dark adaptation at 4 °C from winter to late spring and room temperature in summer. Error bars indicate the mean ± SD (n = 3) for (**a–c**); ± SD (n = 4) for (**d–f**). The statistically significant mean differences (t-test) are marked by asterisks indicating the following confidence intervals: * ≤95%; ** ≤99%.; *** ≤99.9%. Exact p values are provided in the source data file.

(qE/qZ) was slower in the ER samples than in S samples, even after 48 h of recovery, which appears to be mainly due to photoinhibition.

Seasonal changes in the partitioning of absorbed light energy within PSI showed that Y(I) was highest in S, declined in A and W, and reached minimal values in ES (Fig. 2a). Although it decreased, Y(I) was much less affected than the PSII activity (ΦPSII) during the cold periods (Fig. 1f) (Supplementary Fig. 3a). Y(NA) followed the same seasonal pattern, with minimum values registered in ES and a steady recovery until S (Fig. 2b) (Supplementary Fig. 3b). In contrast to Y(NA), Y(ND) considerably increased during the cold periods and peaked (at 69% higher than S values) in ES, then gradually declined to minimum values in S (Fig. 2c, Supplementary Fig. 3c). This suggests that during early spring most of the absorbed light energy is dissipated by oxidized P700 (P700$^+$) to prevent photoinhibition caused by over reduction of the acceptor side as iron-sulfur clusters get damaged[16]. During the first 3 h of the recovery period, ΦPSI did not significantly change, but it gradually returned to S levels over 48 h (Fig. 2d). Y(NA) did not change much during recovery (Fig. 2e). Y(ND) increased slightly during the first 3 h, but then gradually decreased, and ER samples did not quite reach S values. Based on these results, we conclude that the restoration of PSI light use efficiency takes longer than 48 h (Fig. 2f).

Sustained non-photochemical quenching dominates in early spring needles. To elucidate the mechanism of "sustained quenching" observed in pine during the early spring periods, ultrafast time-resolved fluorescence measurements on intact pine

needles were performed using the setup and approach described previously[17,18]. In addition, a special chamber was designed to keep the rotational cuvette with the sample at −20 °C (Supplementary Fig. 4). This chamber was used in order to maintain the "native" sustained quenched state in pine needles. Fluorescence decay traces were collected from pine needles in the same states as reported in the previous subsection: S, ES, ER: Summer needles (S) do not contain any "sustained quenching", while E.spring needles (ES) contain the highest levels of "sustained quenching". To resolve the mechanisms of this quenching, fluorescence decay traces of S needles in the original state (dark-adapted, Fig. 3a, Summer dark) were compared to the needles collected in ES when sustained quenching was present (Fig. 3a, Early spring) and after the quenching in the needles had been relaxed at room temperature (ER) (Fig. 3a, E. spring recovered). To understand whether sustained quenching observed in ES occurs via a similar quenching mechanism to light-induced quenching, S needles exposed to HL for 30 min (SQ) were also measured (Fig. 3a, Summer quenched). As shown by the direct comparison of the decay curves (Fig. 3a), the fluorescence in SQ needles is much shorter-lived as compared to that of S needles. However, the fluorescence decays of ES needles are still pronouncedly shorter-lived than that of the SQ samples, thus characterizing the "sustained quenching" in the ES samples as the most pronounced quenching at all detection wavelengths and under all conditions. In contrast, ER and S samples showed very similar fluorescence decays, indicating that the ES sample recovered quite (although not completely, vide infra) well from sustained quenching within 48 h of recovery treatment.
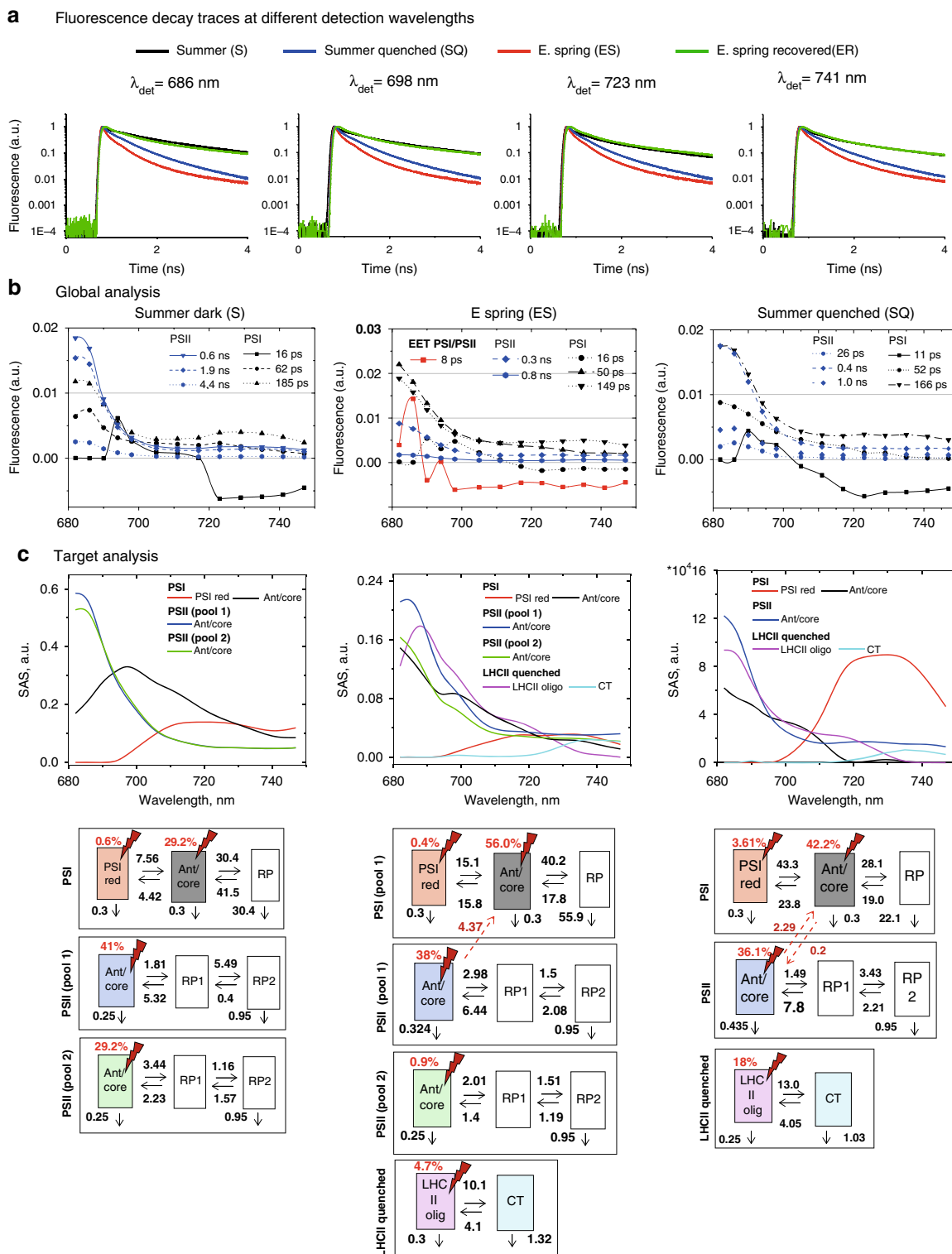
Fig. 3 Time-resolved fluorescence of intact pine needles measured using TCSPC. (a) Fluorescence decay traces measured at −20 °C and at four characteristic wavelengths: 686 nm (mainly PSII, LHCII contributions), 698 nm (PSII, PSI contributions), 723 nm (mainly PSI contribution), and 741 nm (mainly PSI contribution). (**b**) Global analysis of pine needles in three states: Summer dark (S, dark-adapted summer needles, left row), ES (E.spring needles with "sustained quenching" present, middle row), Summer quenched (SQ, right row) (**c**) Kinetic target analysis of pine needles in the three states. See the main text for the explanations. The kinetic target analysis (SAS top, a kinetic model with rate constants in ns-1, bottom) shows the results of the detailed target modeling of the fluorescence kinetics of pine needles. The rate constants (ns^{-1}) and Species-associated emission spectra (SAS) resulted were determined from global target analysis. Species-associated emission spectra (SAS) resulted from the fit of the target kinetic model in the corresponding state. Note that fluorescence decay measurements below 680 nm to detect the decreasing short-wavelength part of the spectra were not possible due to the extremely high scattering of the pine needles. This has no effect however on the ability to distinguish the various lifetime components kinetically and spectrally.

Global analysis of the fluorescence kinetics of pine needles. To get the first hints on the mechanism(s) underlying sustained quenching in early spring global analysis[19] was performed on all datasets: ES, S, SQ (Fig. 3b), and ER (Supplementary Figs. 5–8) needles. Six decay-associated spectra (DAS) were required to fit the fluorescence kinetics in all four cases. Three DAS were tentatively assigned to PSI: 11–16 ps, 50–60 ps, 150–180 ps (Fig. 3b, Supplementary Figs. 5, 6). Their spectra and lifetimes are reminiscent of previously reported PSI-related DAS in other plant species in vivo[17,18,20]. The fastest component represents energy equilibration between Chl_{red} and Chl_{blue}[21,22]. The second DAS in S needles peaks around 685–690 nm with a broad emission in the 700–720 nm region. Therefore, it mainly represents PSI core decay in combination with the 710–720 Chls of Lhcas. The third DAS (185 ps) peaks at 680 nm with some contribution at 730 nm, and therefore, it should be primarily assigned to LHCII and some Chl_{red} in PSI. In quenched states (SQ and ES, in particular) these two DAS have substantially higher contribution around 680 nm and, as a result, the reconstructed steady-state PSI spectra have higher emission around 680–685 nm as compared to the unquenched states (S and ER see Supplementary Fig. 5). It indicates that upon quenching PSII and/or LHCII kinetics also contribute to these PSI-related components. In S and ER states, the remaining three DAS peak at 682 nm and therefore, are assigned to PSII (Fig. 3b and Supplementary Fig. 9). Their lifetimes are 0.5–0.6 ns, 1.5–2.0 ns, and 4 ns, similar to what was resolved previously for PSII in the closed state[17,18]. However, in ES two considerably shorter-lived PSII-related DAS were observed with lifetimes of 0.3 ns and 0.8 ns. This demonstrates that PSII kinetics is indeed quenched strongly in ES needles. Additionally, we resolved a DAS with 8 ps lifetime in the ES sample. The "oscillations" in the spectra giving rise to the sharp bands are due to the mixing of the contributing components, representing excitation energy transfer (EET) from Chl a pools emitting at ~680 nm to those emitting at 690 nm and 700–730 nm, respectively. This suggests that there occurs efficient EET between PSII and/or LHCII and PSI in the ES needles. However, these processes could be unambiguously resolved only by target modeling.

In a nutshell, global analysis results suggest that sustained quenching in the ES state involves both PSII/LHCII and PSI through a direct energy transfer. This mechanism provides much stronger quenching than the high-light-induced quenching in the summer needles (SQ).

Target modeling of the fluorescence kinetics of unquenched pine needles. To resolve the mechanism(s) responsible for the "sustained quenching" in pine needles in detail we performed target analysis[23] of all the kinetic data. In target analysis, a specific kinetic model is tested using a linear time-invariant compartmental model. Each compartment in Fig. 3 is presented by a square box. Each box belongs to any of the three different components: PSI, PSII, LHCII quenched. Fluorescence emitting compartments are presented by colored boxes. The red flashes with numbers directing to that compartments represent the so-called excitation vector, providing the percentage of excitations directed to each compartment and should roughly illustrate the relative number of Chl a (i.e., relative Chl a antenna size) in it. Non-colored boxes represent non-emitting compartments, like radical pairs (RP) in RCs and CT states, which are contributing to the overall observable kinetics and thus have to be included. Target modeling is required to describe the real time-dependent concentrations of each compartment, rates between them (arrows in Fig. 3, ns^{-1}), and spectra (species associated spectra (SAS)) of the interacting components. Note, that the global analysis,

presented in the previous subsection, is equivalent to a number of noninteracting, parallelly decaying compartments and gives only the first indications of the processes involved. It is a mere mathematical analysis, not considering any physical description or information on the studied system. By testing kinetic models that had been validated previously on isolated subcomplexes[24–26] it was possible to separate the PSI from the PSII kinetics. Therefore, our assignment of PSI and PSII is based on a combination of the used kinetic model, resolved rates as well as SAS. The target model and the excitation vector presented in Fig. 3c resulted in the best fitting quality (Supplementary Fig. 7). In S needles (Fig. 3c, Summer dark) the PSI kinetics was described with two emitting compartments (PSI red, Ant/core) and one non-emitting radical pair (RP, Fig. 3c). The resolved rates and SAS are strongly reminiscent of the ones reported for the PSI-LHCI complex[26]. Kinetics from the PSII antenna/RC complex was described by one emitting compartment (Ant/core) and two non-emitting radical pairs (RP1 and RP2, Fig. 3c) as reported previously[17,24,25,27]. According to their SAS and rates, the emitting species represents the equilibrated excited state of the PSII-LHCII super-complex. In our analysis, to achieve a very good fit, two pools of PSII complexes with different decay rates were required (pool 1, pool 2, Fig. 3c, see the detailed comparison of the residuals plots in Supplementary Fig. 7) for the S sample. The two pools differ in the rate constants of charge separation in a manner that is typical for PSII particles with different antenna sizes (see[18,19] for discussion and explanation), which result in different average lifetimes (Supplementary Table 3). In the S sample, PSI with its antenna accounts for 30% of the total absorption cross-section at the excitation wavelength (662 nm), while the two PSII pools account for 40% and 30% of the total absorption cross-section. No internal quenching related to any NPQ process of these PSII compartments was observed.

The target model for the ER needles is rather similar to that of S needles (Supplementary Fig. 5). The main difference is that the smaller PSII pool (with a very small absorption cross-section of ca. 10%) shows an unusually small charge separation rate. The most likely explanation of this phenomenon is a small percentage of PSII RCs has been photoinhibited during the 48 h relaxation process from the sustained quenching state, which agrees with NPQ measurements.

Direct energetic transfer between PSII and PSI is the dominating component of sustained quenching. As for the S samples, also the description of the ES sample (Fig. 3c) required a three-compartmental target model for PSI and the presence of two PSII pools, each described by a three-compartmental model. The two PSII pools differ in the rate constants of charge separation in a similar manner as in S samples. The kinetics are also very similar to that of the S samples, however with a slightly increased charge separation rate. This can be interpreted as a consequence of the partial reduction in the physical antenna size. This goes in line with an increase in the Chl a/b ratio in ES as compared to S samples (Supplementary Fig. 9, Supplementary Table 2). Resolved antenna SAS (Ant/Core compartment of PSI, Fig. 3) of PSI in ES samples contains stronger emission in the 680 nm region, as compared to S needles. That is why we suggest that some LHCII strongly coupled to PSI contribute to it, like recently reported[20].

The striking feature is the presence of a very strong contribution of a direct energy transfer from PSII to PSI. Without allowing for this direct energy transfer, the data could not at all be fitted adequately (Supplementary Figs. 6, 7). This process has a transfer rate of 4.4 ns^{-1}. A small compartment representing quenched and functionally detached LHCII was also

needed for a satisfactory description of the ES samples (See more details on this component in the next section). Overall, the target analysis shows that direct energy transfer from PSII to PSI complexes provides the dominant quenching mechanism of PSII complexes in ES needles causing the pronounced "sustained quenching".

Comparison of sustained quenching and light-induced quenching. To model the fluorescence kinetics of SQ needles again three-compartmental models for PSI and PSII were required. However, unlike in previous cases, one single PSII pool was sufficient to describe the PSII kinetics.

Besides PSII and PSI, one additional component was needed to satisfactorily describe the fluorescence kinetics in the SQ samples. The rates, spectra, and average lifetime (0.4 ns, Supplementary table 3) of these compartments are strongly reminiscent of what was reported previously for highly quenched LHCII aggregates[28], and the quenched LHCII complexes under NPQ conditions in wild type *Arabidopsis*[17] and in *Arabidopsis* mutants depleted of the reaction centers[29]. We, therefore, assign this highly quenched component to the quenched LHCII antenna energetically disconnected from both PSII and PSI. However, the addition of this quenched LHCII compartment was not sufficient to fully describe the fluorescence kinetics (Supplementary Fig. 7). The species-associated spectra (SAS) and kinetics of PSII still contained a substantial amount of 690–700 and 730 nm emission, entirely uncharacteristic for PSII super-complexes, but characteristic of PSI complexes[22,26]. Interestingly, also the SAS of the PSI antenna/core complex contains a 680 nm emission, which is characteristic of PSII. This strongly suggests—as can be directly deduced from the spectral properties—the presence of direct energetic contact between PSI and PSII (Fig. 3c). Introducing such a connection in the target model indeed resulted in a considerably better fit (χ^2 decreased from 1.198 to 1.093, Supplementary Fig. 6). Also, the PSII and PSI kinetics became well-separated in such a model. The resolved direct energy transfer rate from PSII to PSI is quite high (2.3 ns^{-1}), implying that a part of energy absorbed by PSII is actually funneled to PSI. However, this rate of direct energy transfer in SQ needles is only about half of that in ES needles, suggesting that unlike in cold-induced sustained quenching, upon light illumination, spillover is not the major process. The contribution of the quenched antenna, on the other hand, plays a major role.

Efficiency of direct energy transfer quenching in different conditions. By evaluating the kinetic information provided in Fig. 3c one can get a quantitative estimation of the degrees of light use efficiencies (for photosynthesis) on the one hand, and for photoprotection/quenching on the other hand, present in both PSII and PSI in the different situations (c.f. Supplementary Fig. 8, Supplementary Table 4). In S needles 70% of the total absorbed energy drives PSII charge separation and only 30% PSI charge separation. In the SQ needles the percentage of energy flowing into the PSII reaction center drops to 7.1%, while it increases to 67% for PSI. Upon strong light illumination, most of the PSII reaction centers will be closed, and a fraction of that total energy flowing through the RC can produce harmful reactive species like ROS[30,31]. Since the percentage of energy flow into PSII decreases 10 times (70% in S and 7.1% in SQ) in SQ as compared to S, this means that the potential of oxidative damage is reduced by a factor of 10 by the quenching process. This factor is increased by a further factor of approx. 2 due to the large pool of functionally detached and quenched LHCII. So, in SQ needles the overall quenching provides a protection factor of 20 for PSII compared to

S needles. In the sustained quenched ES samples this effect is much more extreme: Only 1.5% of the total absorbed energy in the system flows through the PSII reaction center potentially causing oxidative damage (assuming all other factors are equal). Thus, in total, "sustained quenching" in ES samples provides a protection factor of approx. 40 to PSII (double of SQ) compared to S needles. This huge protection factor explains well why "sustained quenching" is so effective enabling pine needles to survive the harsh winter and early spring conditions.

Massive destacking of grana membranes in the winter. In accordance with early reports[32,33], we observed strong seasonal changes in chloroplast ultrastructure, including loss of grana stacks during early spring (Fig. 4a). Ultrastructural changes derived from morphometric analysis of electron micrographs (Fig. 4a) indicate that average numbers of grana per chloroplast steadily decreased from autumn to winter and reached minimal values in early spring, corresponding to just 68% of S values (Supplementary Table 1). More strikingly, the number of appressed thylakoid layers/granum dramatically declined from A (4.97) to ES (2.72) and rose back in S (6.50) (Supplementary Table 1). These changes corroborate the shift in grana stacking illustrated in Fig. 4b. In S and A, 3–6 layered grana stacks accounted for 60–70% of total stacks. In contrast in ES samples, 70–75% and 15–20% of the grana had only two and three layers, respectively (Fig. 4b). These changes in ES samples were accompanied by a transient doubling of the number of lipid globules (plastoglobuli) per cell (Supplementary Table 1) when the chloroplast structure deviated most strongly from the S state.

To obtain a deeper understanding of the thylakoid plasticity in ES needles we also subjected needles collected at specific early spring and summer dates to EM analysis after artificially induced recovery under different light conditions (Fig. 5a). When both S and ER samples were exposed to HL for 30 (SQ1 for S samples, ERQ1 for ER samples) and 60 min (SQ2 for S samples, ERQ2 for ER samples) similar destacking of grana (as of ES samples) have been observed (Fig. 5b). These changes in grana structures recorded in ER and S samples (Fig. 5c, d) following short term HL exposure strongly corroborate the high dynamic plasticity of the thylakoid membrane, which appears to be essential for acclimation to the harsh boreal winters.

Changes in pigment and protein composition of ES, ER, SQ, and S samples. We also analyzed pigments of the pine needles used for spectroscopic measurements and found substantial differences in pigment contents between S and ES needles (Supplementary Table 2). In S and ES samples the Chl a/b ratios were 2.8 and 3.4, respectively, indicating that S needles had higher relative amounts of Lhcbs and other Chl b-binding proteins. The Chl/carotenoid ratio was also substantially lower in ES samples than in S samples, indicating that they had higher amounts of carotenoids (mainly lutein and violaxanthin/zeaxanthin). We observed no significant difference in total Chl pigment contents between S and SQ samples.

For quantifying the core and antenna proteins, isolated thylakoids were subjected to SDS-PAGE and were immunoblotted against specific antibodies (Supplementary Fig. 9). This revealed that ES samples contain a lower abundance of core (PsaD, PsbD) and antenna (Lhcb2, Lhca4) proteins than in S, in line with earlier reports[34] (Supplementary Fig. 9). ER samples contained lower amounts of PsbD and Lhcb2 compared to S, which might reflect on the minor amount of photoinhibition seen in fluorescence data.
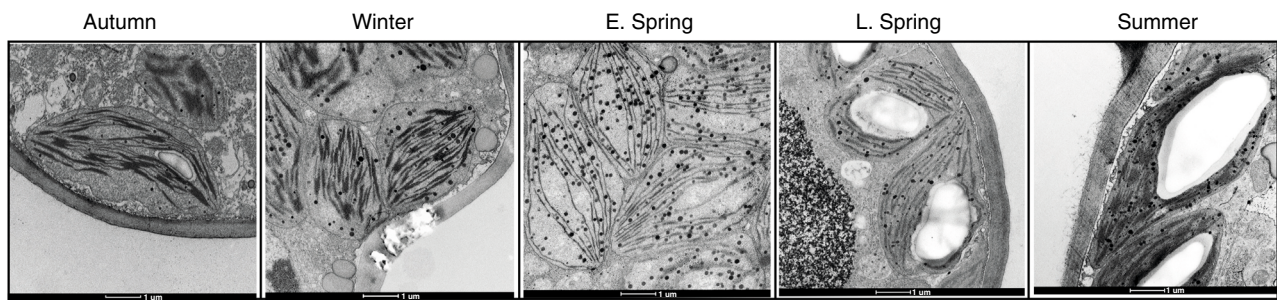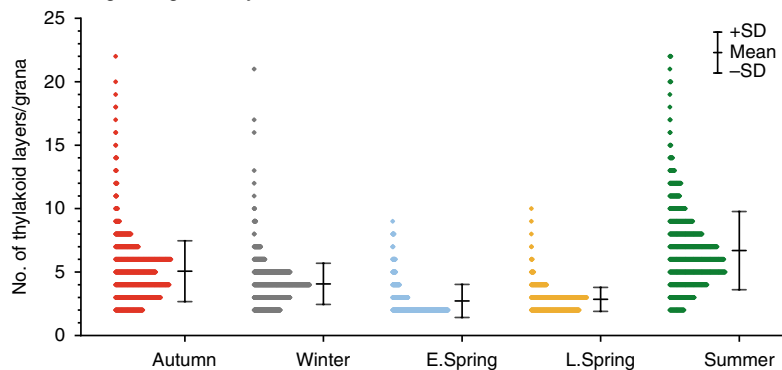
a Seasonal changes in chloroplast ultrastructure

b Changes in grana thylakoids

Fig. 4 Transmission electron microphotographs depicting seasonal variations in chloroplast ultrastructure in pine needles. a Chloroplast structure in Autumn, Winter, E. Spring, L. Spring, and Summer. **b** Histograms of frequency distributions of numbers of thylakoids per granum during the five distinct seasonal periods. The histograms were calculated from 80–100 electron micrographs per season, representing 2–3 chloroplasts per image [Error bars indicate mean ± SD calculated from $n = 1124$ (Autumn), 1235 (Winter), 521 (Early Spring), 578 (Late Spring) and 1048 (Summer) of grana stacks].

Discussion

Distinct changes in chloroplast ultrastructure, including loss of grana thylakoids and disorganization resulting in mostly single-/bi-stromal thylakoid membranes during the cold winter season, followed by recovery during the late spring/summer season have been observed in various conifers[8,13,33]. We observed similar strong seasonal variations in the chloroplast architecture of pine chloroplasts (Fig. 4, Supplementary Table 1), and together with the fluorescence data presented above we are able to decipher the major molecular mechanism that connects these changes to the pronounced 'sustained quenching' described in conifers in the winter.

The seasonal reductions in the maximal quantum efficiency of PSII (Fig. 1e) and light energy utilization during the winter (Fig. 1f) were associated with a substantial increase in excitation pressure, indicating overall reduction of the photosynthetic electron transport chain[35]. In early spring, conifers harvest light energy but the use of the excitation energy for photosynthesis is severely restricted, resulting in potential photoinhibition. Hence, all overwintering conifers must develop highly efficient mechanisms for photoprotection of the photosynthetic apparatus. The major photoprotective mechanism for de-excitation of excess light energy in green plants and algae is the rapidly/ reversible ΔpH- dependent non-photochemical quenching (qE) that occurs in the pigment bed of LHCII proteins[3,17,36]. However, several alternative and/or supplementary photoprotective mechanisms for effective thermal deactivation of excess light energy have also been proposed[5,12,13,37–39].

At first glance, the sharp decline in ΦPSII during early spring (Fig. 1f) might suggest that excess irradiance is dissipated via qE, which has been established as one of the most effective mechanisms for coping with the excess energy flux[3]. However,

fast inducible qE was extremely low (Fig. 1g, h) in ES samples and was not restored to S levels even after 48 h of recovery treatment. (Fig. 1l). This is not unexpected since, in contrast to the fast energy dissipation (qE) depending on ΔpH and PsbS-protein[3] the energy dissipation during winter (sustained quenching) occurs under strong down-regulation, even perhaps in the absence of ΔpH[8,10,40]. However, we can assign this relatively small qE contribution to quench to the small component (accounting for 4.7% of the absorption cross-section) of detached and quenched LHCII. This fraction was much smaller than in light-quenched samples (18%), and absent in both the dark-adapted S samples and recovered ES samples. Incidentally, a so-called "cold hard band" has been reported in low-temperature fluorescence spectra and kinetics of cold-acclimated evergreens[40,41]. Features of this band are reminiscent of quenched LHCII aggregates at low temperature[42], hence it is probably correlated with the fraction of detached and quenched LHCII observed in "sustained quenching" conditions. This led us to conclude that this quenching seen in conifers is not only "Sustained NPQ" but also has a different mechanism.

Detailed quantitative energy partitioning analysis of total absorbed light energy by PSII demonstrates a strong increase (4 fold) of the fraction of constitutive thermal dissipation (ΦNO)[43,44] (Fig. 1i). Usually, this thermal dissipation (ΦNO) contribution is not explained by any clear mechanisms. However, in the case of ES samples, it is strongly suggested by the data that the high levels of ΦNO do reflect the ΔpH-independent "sustained" energy quenching[8,10,40]. Our lifetime data provide an explanation for the origin of this component: A very high rate of direct energy transfer from PSII to PSI, provides this delta-pH independent (non-qE) quenching of PSII. Other photoprotective mechanisms proposed, such as, role of photo-inactivated PSII complexes may also effectively dissipate excess excitation energy as heat[45], and since the
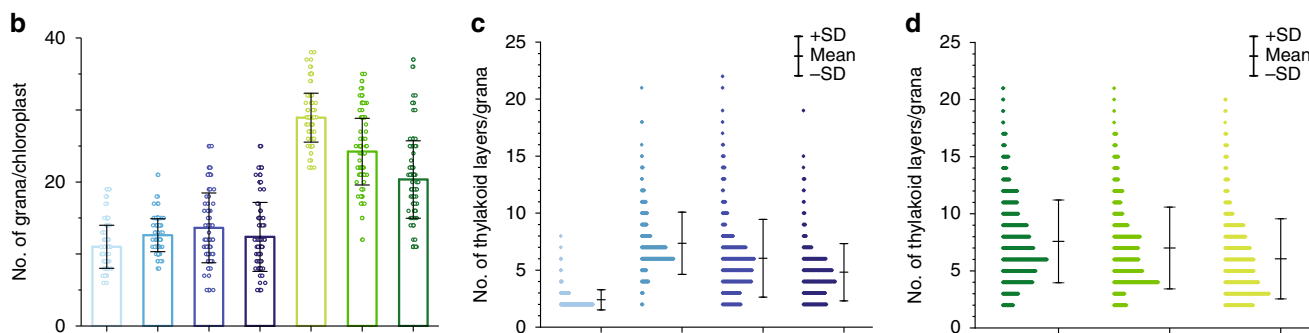
Changes in chloroplast ultrastructure
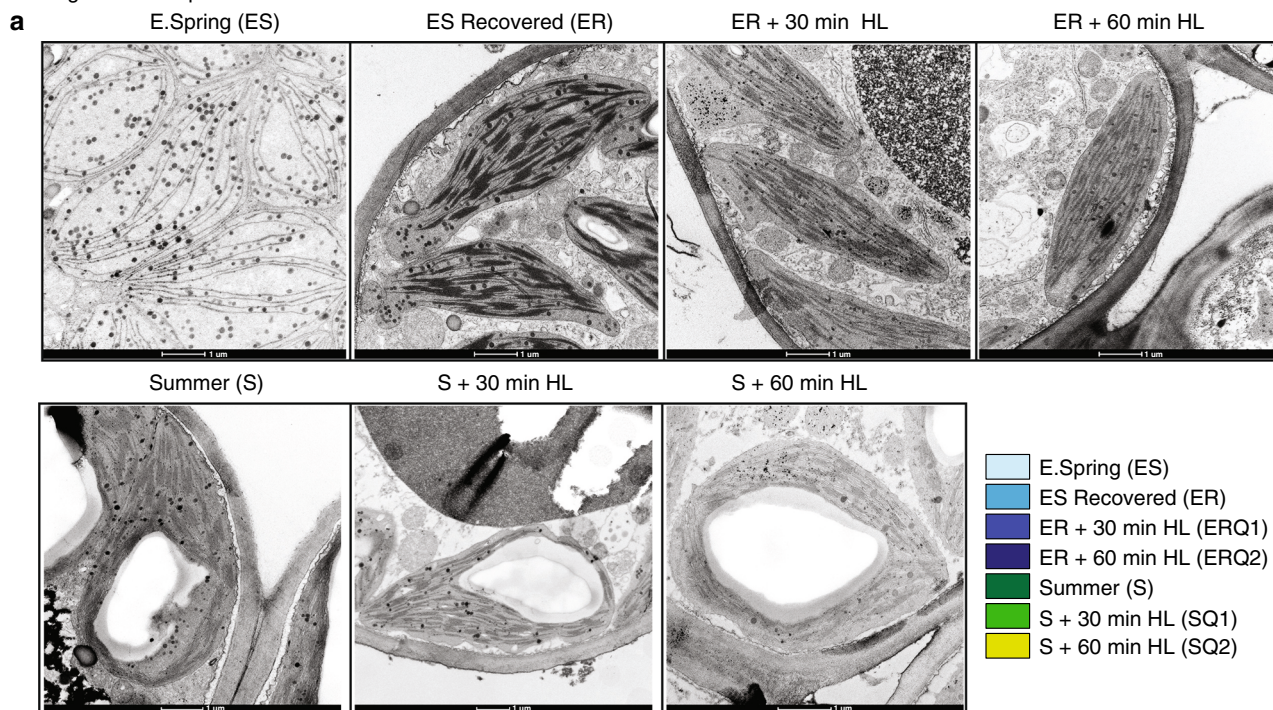
Fig. 5 Artificial induction of changes in chloroplast ultrastructure of pine needles. a Changes in chloroplast ultrastructure in E. spring (ES), E. spring samples recovered (ER) at 18°C for 48 h with a photoperiod of 18 h at 80 μmol m^{-2} s^{-1}, ER samples treated with 800 μmol m^{-2} s^{-1} high light for 30 min (ERQ1), for 60 min (ERQ2). Summer (S), Summer samples treated with 1200 μmol m^{-2} s^{-1} high light for 30 min (SQ1), for 60 min (SQ2). **b** The number of grana per chloroplasts (Error bars indicate mean ± SD ($n = 75$); **c** Histograms of frequency distributions of numbers of thylakoids per granum in different E. spring treated [$n = 220$ (ES), 250 (ER), 272 (ERQ1), 246 (ERQ2)]. **d** Summer treated [$n = 576$ (S), 498 (SQ1), 415 (SQ2)] samples. Error bars indicate the mean ± SD obtained from the analysis of grana stacks.

photoinhibitory quenching (qI), dependent on inactivation and/or degradation of D1, relaxes within hours (or longer), the process could also be considered a form of "sustained quenching". Moreover, the involvement of RC quenching, based on enhanced S_2Q_{A-} and S_2Q_{B-} charge recombination, favoring non-radiative PSII RC dissipation of excess light has been suggested to supplement or even replace the fast component of non-photochemical quenching during winter, and thus play a significant role in overwintering conifers[37,38]. However, we found no indication of photoinhibited PSII centers in the unrelaxed ES samples that displayed sustained quenching. A component with these characteristics was not observed in the ES samples. However, even if it would be present it could not explain the strong quenching effect since this component has a longer average lifetime and higher fluorescence yield than the intact PSII units. In addition, we found no experimental evidence for PSII RC quenching either. All rate constants obtained from target modeling of the PSII antenna/RC pools in both unquenched

and quenched states are quite normal. Thus, neither photoinhibition nor RC quenching alone could explain the strong "sustained quenching". Moreover, changes in Y(I) suggest a lowered activity of PSI, even though PSI activity was less affected than PSII. In the absence of carbon fixation one would expect higher acceptor side limitation, but contrastingly we found Y(NA) less affected and donor side limitation [Y(ND)] was very high (compared to S). This makes sense if PSII directly transfers energy to PSI, making PSI an energy sink for PSII by reducing linear electron flow and in turn, causing PSI donor side limitation (oxidized P700) to increase.

The detailed structural and functional data presented here enable inference of a coherent quenching/photoprotection mechanism involving structural rearrangements of the thylakoids. The model explains Scots pine's acclimation to the combination of harsh freezing temperatures and high solar radiation that occurs during early spring in northern boreal forests (Fig. 6).
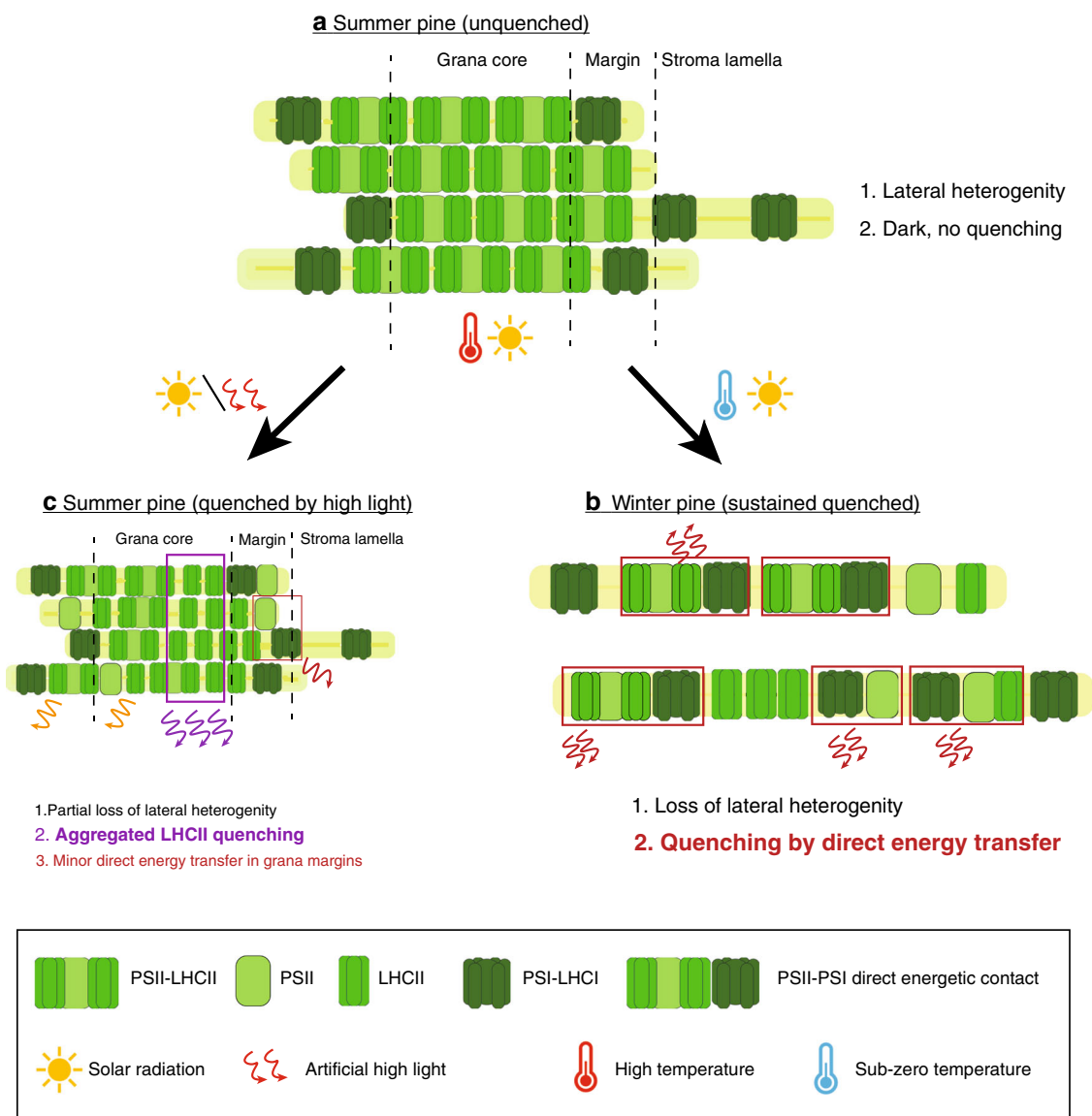
Fig. 6 Molecular model for acclimation of photosynthetic machinery under changing natural environmental conditions. Changes in Summer unquenched (**a**); Winter quenched (**b**); Summer quenched (**c**) in Scots pine. The larger text indicates the process is dominating under that condition. Text colors correspond to the legend colors of the figure.

Acclimation to early spring conditions (Fig. 6b) results in massive loss of grana stacks (destacking) and formation of uniform membrane structures of stromal thylakoids and phosphorylation of Lhcb1 and/or PsbS, that has been identified in Norway spruce, could be a trigger for the process[14]. This allows for a redistribution and randomization of PSII and PSI. The reduction in the spatial distance between PSII and PSI complexes increases the probability of direct energy transfer from PSII to PSI[46–48]. This protective mechanism severely restricts linear electron flow since it strongly quenches PSII activity. It also has strong similarities to the potent quenching observed in other extreme environmental conditions when PSII requires strong protection. Examples include drying-induced quenching in lichen[49] and heat-induced quenching in *Symbiodinium* cells of coral[50]. In both cases, destacking and reorganization of the thylakoid membrane occur, resulting in proximity of PSII to PSI complexes with direct energy transfer.

In conclusion, during early spring only a very small fraction of the absorbed light energy in PSII antennae is utilized for PSII photochemistry (ΦPSII) and the fast inducible NPQ (qE) is low

since it not only requires a high ΔpH[3,6,17] but there is a strong static quenching present already. On the other hand protection from extreme oxidative stress and rearrangement of thylakoid complexes are likely coupled to the high zeaxanthin content[51–53] (Supplementary table 2), and probably to pronounced phosphorylation of antenna and core proteins present under these conditions[54]. In this situation, the excess energy is dissipated primarily through direct energy transfer from PSII to PSI, which appears in steady-state (PAM) fluorescence measurements as a non-regulated constitutive energy quenching. An additional, albeit smaller, amount of quenching and photoprotection is provided under sustained quenching conditions by the qE mechanism in functionally detached LHCII. It is possible that this fraction is linked to large aggregates containing LHCII, PsbS, and other small proteins, previously detected in cold-adapted pine needles[55]. Thus, conifers appear to have a powerful protective mechanism that resembles those found in other photosynthetic organisms of relatively harsh environments[49,50]. This protective mechanism plays a crucial role in the survival of pine from harsh boreal winters.

Methods

Weather. Weather data were recorded from October 2015 to May 2016, from November 2016 to June 2017, and from October 2017 to June 2018 on an hourly basis at the weather station of the Sweden's meteorological and hydrological institute, Umeå stations. (available on https://www.smhi.se).

Plant material and sampling. Fully developed needles were collected frequently, from Oct 2015 to May 2016, from Nov 2016 to June 2017 and Oct 2017 to June 2018, inclusive, at midday (8.00–10.00) from fully exposed south-facing branches of five Scots pine (*Pinus sylvestris* L.) trees growing on Umeå University campus (63° 49' N, 20° 18' E). The collected needles were immediately stored in darkness, at 0–5 °C, in a laboratory at Umeå Plant Science Centre, and subjected to measurements (described in the following sections) shortly after sampling to minimize any further changes in the photosynthetic machinery. For recovery treatment samples from winter-stressed branches were collected in mid-March and subjected to recovery treatment, involving exposure to very low light (80 μmol photons m^{-2}s^{-1}) at 20 °C[55]. Further details are provided (together with other details regarding the sampling dates and procedures) in Supplementary Fig. 1.

Modulated chlorophyll fluorescence and P700 + measurements. Chlorophyll fluorescence was measured using a Dual-PAM-100 instrument (Heinz Walz GmbH, Effeltrich, Germany) at room temperature (20 °C) after 30 min dark adaptation at low temperature [below 5 °C, winter samples (samples collected during November to May)] (No changes occurred in sustained quenched (E. Spring) samples during the measuring period) or room temperature [(20 °C, summer samples (samples collected during June to October)]. Maximum photochemical efficiency of PSII was calculated as Fv/Fm = (Fm − Fo)/Fm. To perform quantum yield measurements, we chose to record a light response curve where we measured Fv/Fm first, followed by Pm (maximal P700 oxidation), and then changing the actinic light intensity stepwise from 3 μmol photons m^{-2}s^{-1} to 1469 μmol photons m^{-2}s^{-1}. During the recording of light response curves, samples were exposed to each light intensity for 3 min followed by a saturating pulse (SP) of 4000 μmol photons m^{-2}s^{-1} was superimposed in the presence of actinic light to get the maximum chlorophyll fluorescence in light-adapted state (Fm'). All the quantum yields were calculated from the saturating pulse applied after 300 μmol m^{-2} s^{-1} of the light illumination period of the light response curve. Partitioning of absorbed light energy in PSII was estimated as ΦPSII + ΦNPQ + ΦNO = 1[43,44]. Where, ΦPSII is the effective quantum yield of PSII, ΦNPQ is the quantum yield of energy dissipated as regulated NPQ mainly by heat, and ΦNO is the fraction of energy dissipated by other non-regulatory pathways. The effective photochemical quantum yield of PSI, Y(I), was calculated as Y(I) = 1−(Y(ND) + Y(NA))[56]. Here, Y(I) is the effective quantum yield of PSI (ΦPSI) when reaction centers (RCs) are open with reduced donor side (P700) and oxidized acceptor side (A); Y(NA) is the energy dissipation due to acceptor side limitation, reflecting the redox state of the acceptor side when RCs are closed with P700 reduced and both acceptors reduced; and Y(ND) is the energy dissipation due to donor side limitation, reflecting the redox state with both P700 and A oxidized. Steady-state NPQ induction was measured with SP applied under constant actinic light illumination of either 300 (seasonal measurements)/800 (recovery experiment) μmol m^{-2} s^{-1} with saturating pulse applied every 30 s.

Ultrafast fluorescence measurements. Intact needles were subjected to ultrafast time-correlated single-photon counting measurements at −20 °C in a rotating cuvette, as previously described[17,18]. Pine needles were immersed in 60% PEG solution (pH 7.5), which was used as an anti-freeze. Tests confirmed that this solution did not significantly affect either the Fv/Fm values or fluorescence kinetics. These conditions allowed maintenance of the physiological and quenching states for a long time during the measurements and prevention of radiation damage or further quenching induction by the very weak measuring light. Needles sampled in summer (S needles) were measured in both unquenched and fully light-quenched states. For measurement in the unquenched state, they were dark-adapted for 30 min, then quickly frozen to −20 °C in the rotation cuvette. For measurement in the light-quenched state, the needles were illuminated by red light (intensity 1000 μmol m^{-2}sec^{-1}) for 30 min. at room temperature. During this time, fluorescence intensity was monitored and after 30 min a steady-state level was reached. The needles were then frozen quickly under illumination in the rotation cuvette to −20 °C. Early spring samples (ES samples) were measured either in the original "sustained quenching state" by transferring them directly at −20 °C into the cooled rotation cuvette (Supplementary Fig. 4), or in a "recovery state" induced by exposing them to very low light (80 μmol m^{-2}s^{-1}) at 20 °C, as described earlier, then freezing them (as in the measurements of the summer needles in unquenched state). After each fluorescence lifetime measurement, the samples were fast-frozen in liquid nitrogen and stored at −80 °C for further pigment analysis. The laser settings for the measurements were 40–60 μW power, 4 MHz repetition rate, and 1 mm diameter beam size. Excitation wavelength was set to 662 nm to excite Qy band of Chl *a* in order to resolve fluorescence kinetics by sufficiently advanced kinetic target models established previously[25,28,30] without their further

overcomplication. Soret band excitation or Chl *b* excitation would result in substantially more complex fluorescence kinetics than the one observed here due to the contribution of Soret→Qy deactivation and Chl *b* → Chl *a* energy transfer pathways, which have multiexponential character[57–60]. Furthermore, usage of excitation wavelengths further from Boltzmann equilibrium at 665–670 nm, would result in the necessity to include complex equilibration kinetics[61].

Pigment and protein analysis. Pigments were extracted from frozen pine needles with 80% acetone. Chl a/b and Chl/carotenoid ratios were calculated by fitting the extracts' absorption spectra with the spectra of the individual pigments, and the relative amounts of carotenoids were determined by HPLC[62]. First acetone extracts (~200 μL, Qy OD 0.3–0.8/cm) of the needles were loaded on a SephereClone 5 u ODS1 column (Phenomenex) with a 1.5 mL/min flow rate. Buffer A composition was acetonitrile/methanol/0.1 M Tris-HCl pH 7.6 in 72:8:10 ratio. Buffer composition was methanol/hexane in 4:1 ratio. The amount of buffer B was linearly increased to 50% in 10 min, held at this value for 0.5 min, and then increased linearly to 100% in 4 min. Thylakoid membranes for SDS-PAGE protein composition analysis were isolated from fully developed Pinus sylvestris needles using three different buffers. First, needles were homogenized in grinding buffer (50 mM Hepes–KOH, pH 7.5; 330 mM sorbitol; 5 mM MgCl₂; 10 mM NaF; 10% (w/v) polyethylene glycol, 6000 kDa; 0.075% (w/v) bovine serum albumin; 0.065% (w/v) Na-ascorbate) in a blender (Multiblender Coline, Clas Ohlson), followed by filtering through two layers of Miracloth (VWR, MiliporeSigma, #EM475855-1R). The filtered homogenate was centrifuged at 6000 g for 6 min. The pellet was resuspended in a medium containing: 50 mM Hepes–KOH, pH 7.5; 5 mM MgCl₂; 10 mM NaF and centrifuged as above. The pelleted thylakoid membranes were resuspended again in storage buffer (50 mM Hepes–KOH, pH 7.5; 5 mM MgCl₂; 10 mM sorbitol; 10 mM NaF), frozen in small aliquots and stored in −80 °C for further use[63]. Thylakoid membranes containing equal amounts of protein were subjected to SDS-PAGE separation[64] using Criterion TGX Any kD™ precasted gels (BioRad, #5678124) and electrophoretically transferred to a PVDF membrane (BioRad, #1704156) using Trans-Blot® Turbo™ Transfer System (BioRad, #1704150). Membranes were probed with specific primary antibodies against: PsbD (1:5000 dilution), PsaD (1:10000 dilution), Lhcb2 (1:15000 dilution) and Lhca4 (1:15000 dilution). After incubation with horseradish peroxidase-conjugated secondary antibody (Goat anti-Rabbit IgG (H&L), #AS09 602, all antibodies from Agrisera AB, Vännäs, Sweden) the antibody complexes were visualized by incubation of the blots in Agrisera ECL chemiluminescent detection set (#AS16 ECL-S-N) (as per manufacturer's instructions) in Azure c600 developing device (Azure Bioscience, USA)

Transmission electron microscopy. Thin slices (< 0.5 mm) from the middle region of pine needles were cut in tap water and fixed in 4% paraformaldehyde, 2.5% glutaraldehyde (TAAB Laboratories, Aldermaston, England) in 0.1 M or 0.05 M (May and June) sodium cacodylate buffer, pH 7.4 (TAAB Laboratories, Aldermaston, England). Thoroughly washed samples were post-fixed in 1% osmium tetroxide (TAAB Laboratories, Aldermaston, England). The fixed material was dehydrated in ethanol series with increasing concentrations and propylene oxide and finally embedded in Spurr resin (TAAB Laboratories, Aldermaston, England). Ultrathin sections (70 nm) were post contrasted in uranyl acetate and Reynolds lead citrate and further examined with Talos 120 C electron microscope (FEI, Eindhoven, The Netherlands) operating at 120 kV. Micrographs were acquired with a Ceta 16 M CCD camera (FEI, Eindhoven, The Netherlands) using TEM Image & Analysis software ver. 4.14 (FEI, Eindhoven, The Netherlands). The chloroplast ultrastructure was analyzed from the electron micrographs by measuring the average number of chloroplasts per cell, average number of grana per chloroplasts and average number of appressed thylakoids per grana stack (Ng)[65,66].

Statistical analysis. The significance of between-mean differences was assessed by t-tests and p values were recorded. One (*), two (**), and three (***) asterisks in the presented figures indicate *≤95%; **≤99%; ***≤99.9% confidence levels, respectively, for fluorescent and electron microscopic measurements.

Reporting summary. Further information on research design is available in the Nature Research Reporting Summary linked to this article.

Data availability

Source and raw data for Figs. 1, 2, 4, and 5 are provided in the source data file. Source data for Fig. 3 is provided in the manuscript. Source data for Supplementary Figs. 2, 3, 4, 5, 6, 7, 8, and 9 are provided in the source data file. Representative electron micrographs in Figs. 4 and 5 are provided in the manuscript, all other electron micrographs which were analyzed to obtain the graphs in Figs. 4 and 5 can be provided upon reasonable request. All Source data are provided with this paper.

References

1. Gowthrop D. *Vanishing Halo*. Greystone Books; 2009. https://books.google.se/books?id=t-SDCgAAQBAJ.
2. Nystedt, B. et al. The Norway spruce genome sequence and conifer genome evolution. *Nature* **497**, 579–584 (2013).
3. Li, X.-P. et al. A pigment-binding protein essential for regulation of photosynthetic light harvesting. *Nature* **403**, 391–395 (2000).
4. Jahns, P. & Holzwarth, A. R. The role of the xanthophyll cycle and of lutein in photoprotection of photosystem II. *Biochim Biophys. Acta-Bioenerg.* **1817**, 182–193 (2012).
5. Malnoë, A. Photoinhibition or photoprotection of photosynthesis? Update on the (newly termed) sustained quenching component qH. *Environ. Exp. Bot.* **154**, 123–133 (2018).
6. Niyogi, K. K. Photoprotection revisited: genetic and molecular approaches. *Annu Rev. Plant Biol.* **50**, 333–359 (1999).
7. Horton, P., Ruban, A. V. & Walters, R. G. Regulation of light harvesting in green plants. *Annu Rev. Plant Biol.* **47**, 655–684 (1996).
8. Öquist, G. & Huner, N. P. A. Photosynthesis of overwintering evergreen plants. *Annu. Rev. Plant Biol.* **54**, 329–355 (2003).
9. Yang, Q. et al. Two dominant boreal conifers use contrasting mechanisms to reactivate photosynthesis in the spring. *Nat. Commun.* **11**, 1–12 (2020).
10. Verhoeven, A. Sustained energy dissipation in winter evergreens. *N. Phytol.* **201**, 57–65 (2014).
11. Harsch, M. A., Zhou, Y., HilleRisLambers, J. & Kot, M. Keeping pace with climate change: stage-structured moving-habitat models. *Am. Nat.* **184**, 25–37 (2014).
12. Demmig-Adams, B. & Adams, W. W. III Photoprotection in an ecological context: the remarkable complexity of thermal energy dissipation. *N. Phytol.* **172**, 11–21 (2006).
13. Krol, M. et al. Low growth temperature inhibition of photosynthesis in cotyledons of jack pine seedlings (Pinus banksiana) is due to impaired chloroplast development. *Can. J. Bot.* **80**, 1042–1051 (2002).
14. Grebe, S. et al. Specific thylakoid protein phosphorylations are prerequisites for overwintering of Norway spruce (Picea abies) photosynthesis. *Proc. Natl Acad. Sci. USA* **117**, 17499–17509 (2020).
15. Genty, B., Briantais, J. M. & Baker, N. R. The relationship between the quantum yield of photosynthetic electron transport and quenching of chlorophyll fluorescence. *Biochim Biophys. Acta* **990**, 87–92 (1989).
16. Tiwari, A. et al. Photodamage of iron–sulphur clusters in photosystem I induces non-photochemical energy dissipation. *Nat. Plants* **2**, 1–9 (2016).
17. Holzwarth, A. R., Miloslavina, Y., Nilkens, M. & Jahns, P. Identification of two quenching sites active in the regulation of photosynthetic light-harvesting studied by time-resolved fluorescence. *Chem. Phys. Lett.* **483**, 262–267 (2009).
18. Chukhutsina, V. U., Holzwarth, A. R. & Croce, R. Time-resolved fluorescence measurements on leaves: principles and recent developments. *Photosynth Res.* **140**, 355–369 (2019).
19. Van Stokkum, I. H. M., Larsen, D. S., Van & Grondelle, R. Global and target analysis of time-resolved spectra. *Biochim Biophys. Acta-Bioenerg.* **1657**, 82–104 (2004).
20. Chukhutsina V. U., Liu Xin, Xu Pengqi CR. The major light-harvesting complex (LHCII) is an antenna of photosystem I in dark-adapted plants. *Nat Plants*. Published online 2020. https://doi.org/10.1038/s41477-020-0693-4.
21. Croce, R., Dorra, D., Holzwarth, A. R. & Jennings, R. C. Fluorescence decay and spectral evolution in intact photosystem I of higher plants. *Biochemistry* **39**, 6341–6348 (2000).
22. Wientjes, E., Van Stokkum, I. H. M., Van Amerongen, H. & Croce, R. Excitation-energy transfer dynamics of higher plant photosystem I light-harvesting complexes. *Biophys. J.* **100**, 1372–1380 (2011).
23. Holzwarth A. R. Data analysis of time-resolved measurements. In: *Biophysical Techniques in Photosynthesis*. Springer; 1996:75–92.
24. Holzwarth, A. R., Müller, M. G., Niklas, J. & Lubitz, W. Ultrafast transient absorption studies on photosystem I reaction centers from Chlamydomonas reinhardtii. 2: mutations near the P700 reaction center chlorophylls provide new insight into the nature of the primary electron donor. *Biophys. J.* **90**, 552–565 (2006).
25. Miloslavina, Y. et al. Charge separation kinetics in intact photosystem II core particles is trap-limited. A picosecond fluorescence study. *Biochemistry* **45**, 2436–2442 (2006).
26. Slavov, C., Ballottari, M., Morosinotto, T., Bassi, R. & Holzwarth, A. R. Trap-limited charge separation kinetics in higher plant photosystem I complexes. *Biophys. J.* **94**, 3601–3612 (2008).
27. Szczepaniak, M. et al. Charge separation, stabilization, and protein relaxation in photosystem II core particles with closed reaction center. *Biophys. J.* **96**, 621–631 (2009).
28. Miloslavina, Y. et al. Far-red fluorescence: A direct spectroscopic marker for LHCII oligomer formation in non-photochemical quenching. *FEBS Lett.* **582**, 3625–3631 (2008).
29. Ware, M. A., Giovagnetti, V., Belgio, E. & Ruban, A. V. PsbS protein modulates non-photochemical chlorophyll fluorescence quenching in membranes depleted of photosystems. *J. Photochem Photobiol. B Biol.* **152**, 301–307 (2015).
30. Lambrev, P. H., Miloslavina, Y., Jahns, P. & Holzwarth, A. R. On the relationship between non-photochemical quenching and photoprotection of photosystem II. *Biochim. Biophys. Acta-Bioenerg.* **1817**, 760–769 (2012).
31. Khorobrykh, S., Havurinne, V., Mattila, H. & Tyystjärvi, E. Oxygen and ROS in Photosynthesis. *Plants* **9**, 91 (2020).
32. Parker, J. & Philpott, D. E. An electron microscopic study of chloroplast condition in summer and winter in Pinus strobus. *Protoplasma* **53**, 575–583 (1961).
33. Martin, B. & Öquist, G. Seasonal and experimentally induced changes in the ultrastructure of chloroplasts of Pinus silvestris. *Physiol. Plant.* **46**, 42–49 (1979).
34. Verhoeven, A., Osmolak, A., Morales, P. & Crow, J. Seasonal changes in abundance and phosphorylation status of photosynthetic proteins in eastern white pine and balsam fir. *Tree Physiol.* **29**, 361–374 (2009).
35. Huner, N. et al. Chloroplast redox imbalance governs phenotypic plasticity: the "grand design of photosynthesis" revisited. *Front Plant Sci.* **3**, 255 (2012).
36. Nilkens, M. et al. Identification of a slowly inducible zeaxanthin-dependent component of non-photochemical quenching of chlorophyll fluorescence generated under steady-state conditions in Arabidopsis. *Biochim Biophys. Acta-Bioenerg.* **1797**, 466–475 (2010).
37. Ivanov, A. et al. Seasonal responses of photosynthetic electron transport in Scots pine (Pinus sylvestris L.) studied by thermoluminescence. *Planta* **215**, 457–465 (2002).
38. Sveshnikov, D. et al. Excitation energy partitioning and quenching during cold acclimation in Scots pine. *Tree Physiol.* **26**, 325–336 (2006).
39. Tikkanen, M. & Aro, E.-M. Integrative regulatory network of plant thylakoid energy transduction. *Trends Plant Sci.* **19**, 10–17 (2014).
40. Gilmore, A. M. & Ball, M. C. Protection and storage of chlorophyll in overwintering evergreens. *Proc. Natl Acad. Sci. USA* **97**, 11098–11101 (2000).
41. Gilmore, A. M., Matsubara, S., Ball, M. C., Barker, D. H. & Itoh, S. Excitation energy flow at 77 K in the photosynthetic apparatus of overwintering evergreens. *Plant Cell Environ.* **26**, 1021–1034 (2003).
42. Ostroumov E. E., Götze J. P., Reus M., Lambrev P. H., Holzwarth A. R. Characterization of fluorescent chlorophyll charge-transfer states as intermediates in the excited state quenching of light-harvesting complex II. *Photosynth Res.* **144**, 1–23 (2020).
43. Kramer, D. M., Johnson, G., Kiirats, O. & Edwards, G. E. New fluorescence parameters for the determination of Q A redox state and excitation energy fluxes. *Photosynth Res.* **79**, 209 (2004).
44. Hendrickson, L., Furbank, R. T. & Chow, W. S. A simple alternative approach to assessing the fate of absorbed light energy using chlorophyll fluorescence. *Photosynth Res.* **82**, 73 (2004).
45. Krause, G. H. Photoinhibition of photosynthesis. An evaluation of damaging and protective mechanisms. *Physiol. Plant.* **74**, 566–574 (1988).
46. Barber, J. An explanation for the relationship between salt-induced thylakoid stacking and the chlorophyll fluorescence changes associated with changes in spillover of energy from photosystem II to photosystem I. *FEBS Lett.* **118**, 1–10 (1980).
47. Barber, J. Influence of surface charges on thylakoid structure and function. *Annu. Rev. Plant Physiol.* **33**, 261–295 (1982).
48. Barber, J. Photosynthetic energy conversion: natural and artificial. *Chem. Soc. Rev.* **38**, 185–196 (2009).
49. Slavov, C., Reus, M. & Holzwarth, A. R. Two different mechanisms cooperate in the desiccation-induced excited state quenching in Parmelia lichen. *J. Phys. Chem. B.* **117**, 11326–11336 (2013).
50. Slavov, C. et al. "Super-quenching" state protects Symbiodinium from thermal stress—implications for coral bleaching. *Biochim Biophys. Acta-Bioenerg.* **1857**, 840–847 (2016).
51. Vajravel, S. et al. Zeaxanthin and echinenone modify the structure of photosystem I trimer in Synechocystis sp. PCC 6803. *Biochim Biophys. Acta-Bioenerg.* **1858**, 510–518 (2017).
52. Tian, L., Xu, P., Chukhutsina, V. U., Holzwarth, A. R. & Croce, R. Zeaxanthin-dependent nonphotochemical quenching does not occur in photosystem I in the higher plant Arabidopsis thaliana. *Proc. Natl Acad. Sci. USA* **114**, 4828–4832 (2017).
53. HavauxM., Dall'OstoL. & BassiR. Zeaxanthin has enhanced antioxidant capacity with respect to all other xanthophylls in arabidopsis leaves and functions independent of binding to PSII antennae. *Plant Physiol.* **145**, 1506–1520 (2007).
54. Merry, R., Jerrard, J., Frebault, J. & Verhoeven, A. A comparison of pine and spruce in recovery from winter stress; changes in recovery kinetics, and the abundance and phosphorylation status of photosynthetic proteins during winter. *Tree Physiol.* **37**, 1239–1250 (2017).

55. Ottander, C., Campbell, D. & Öquist, G. Seasonal changes in photosystem II organisation and pigment composition in Pinus sylvestris. *Planta* **197**, 176–183 (1995).
56. Schreiber, U. Saturation pulse method for assessment of energy conversion in PSI. *PAM Appl Notes* **1**, 11–14 (2008).
57. Gradinaru, C. C. et al. The flow of excitation energy in LHCII monomers: implications for the structural model of the major plant antenna. *Biophys. J.* **75**, 3064–3077 (1998).
58. Gradinaru, C. C. et al. Ultrafast evolution of the excited states in the chlorophyll a/b complex CP29 from green plants studied by energy-selective pump−probe spectroscopy. *Biochemistry* **37**, 1143–1149 (1998).
59. Gradinaru C. C., van Stokkum I. H. M., van Grondelle R., van Amerongen H. Ultrafast Absorption Changes of the Lhcii Carotenoids upon Selective Excitation of the Chlorophylls BT - Photosynthesis: Mechanisms and Effects: Volume I–V: Proceedings of the XIth International Congress on Photosynthesis, Budapest, Hungary, August 17–22. In: Garab G., ed. Springer Netherlands; 1998:277–280. https://doi.org/10.1007/978-94-011-3953-3_64.
60. Connelly, J. P., Müller, M. G., Bassi, R., Croce, R. & Holzwarth, A. R. Femtosecond transient absorption study of carotenoid to Chlorophyll energy transfer in the light-harvesting complex II of photosystem II. *Biochemistry* **36**, 281–287 (1997).
61. van Grondelle, R., Bergström, H., Sundström, V. & Gillbro, T. Energy transfer within the bacteriochlorophyll antenna of purple bacteria at 77 K, studied by picosecond absorption recovery. *Biochim Biophys. Acta - Bioenerg.* **894**, 313–326 (1987).
62. Xu, P., Tian, L., Kloz, M. & Croce, R. Molecular insights into Zeaxanthin-dependent quenching in higher plants. *Sci. Rep.* **5**, 1–10 (2015).
63. Grebe, S. et al. The unique photosynthetic apparatus of Pinaceae: analysis of photosynthetic complexes in Picea abies. *J. Exp. Bot.* **70**, 3211–3225 (2019).
64. Damkjær, J. T. et al. The photosystem II light-harvesting protein Lhcb3 affects the macrostructure of photosystem II and the rate of state transitions in Arabidopsis. *Plant Cell.* **21**, 3245–3256 (2009).
65. Ivanov, A. G., Ignatova, N. S. & Christov, A. M. Comparative ultrastructural and fluorescence studies of grapevine (Vitis vinifera L.) chloroplasts isolated from stem and leaf tissues. *Plant Sci.* **67**, 253–257 (1990).
66. Ivanov, A. G., Kitcheva, M. I., Christov, A. M. & Popova, L. P. Effects of abscisic acid treatment on the thermostability of the photosynthetic apparatus in barley chloroplasts. *Plant Physiol.* **98**, 1228–1232 (1992).

Acknowledgements

Author contributions

Funding

Competing interests
The authors declare no competing interests.

Additional information
Supplementary information is available for this paper at https://doi.org/10.1038/s41467-020-20137-9.

Correspondence and requests for materials should be addressed to A.R.H. or S.J.

Peer review information *Nature Communications* thanks the anonymous reviewers for their contribution to the peer review of this work. Peer review reports are available.

Reprints and permission information is available at http://www.nature.com/reprints

Publisher's note Springer Nature remains neutral with regard to jurisdictional claims in published maps and institutional affiliations.